On the width-amplitude inequality of electron phase space holes

Li-Jen Chen and Jolene Pickett
Department of Physics and Astronomy, University of Iowa, Iowa City, Iowa, USA

Paul Kintner and Jason Franz
School of Electrical Engineering, Cornell University, Ithaca, New York, USA

Donald Gurnett
Department of Physics and Astronomy, University of Iowa, Iowa City, Iowa, USA

Received 17 February 2005; revised 25 April 2005; accepted 17 July 2005; published 9 September 2005.

[1] Electron phase space holes are analyzed in terms of solitary-wave solutions to the nonlinear Vlasov-Poisson equations in a collisionless plasma. Width-amplitude relations for one-dimensional and three-dimensional electron holes are derived to be inequalities that allow existence of the holes in regions to one side of a bound. The theoretical origin of the width-amplitude inequality is elucidated to show that the inequality nature is independent of specific functional forms of the solitary potential and ambient plasma distribution functions. Ion dynamics and effects of finite hole velocity and finite perpendicular size are subsequently included. Finally, we show that the electron holes reported by Franz et al. (2005) populate an allowed region in the solution space that is significantly away from the bounding curve. These electron holes evidence the accessibility of electron holes whose widths and amplitudes are only loosely constrained and open up the possibility of spontaneous generation of phase-space holes in turbulent fluctuations.

Citation: Chen, L.-J., J. Pickett, P. Kintner, J. Franz, and D. Gurnett (2005), On the width-amplitude inequality of electron phase space holes, *J. Geophys. Res.*, *110*, A09211, doi:10.1029/2005JA011087.

1. Introduction

[2] Electrostatic solitary waves have been observed ubiquitously in space [*Temerin et al.*, 1982; *Boström et al.*, 1988; *Matsumoto et al.*, 1994; *Mozer et al.*, 1997; *Franz et al.*, 1998; *Ergun et al.*, 1998; *Tsurutani et al.*, 1998; *Bale et al.*, 1998; *Kojima et al.*, 1999; *Bounds et al.*, 1999; *McFadden et al.*, 2003; *Pickett et al.*, 2003; *Cattell et al.*, 2003; *Pickett et al.*, 2004a, 2004b, and references therein] and heliospheric [*Mangeney et al.*, 1999; *Williams et al.*, 2005] plasmas. For the cases when the widths and amplitudes of the solitary potentials can be determined experimentally, phase space electron or ion holes are shown to be the best candidates for the observed structures [*Franz et al.*, 1998; *Ergun et al.*, 1998, 1999; *Cattell et al.*, 1999; *Bounds et al.*, 1999; *Franz et al.*, 2000; *McFadden et al.*, 2003; *Behlke et al.*, 2004]. One-dimensional theories for electron holes have different conclusions on the width-amplitude relation. Among them are that the potential width must increase with increasing amplitudes [*Turikov*, 1984; *Muschietti et al.*, 1999a, 1999b, 1999c], the width decreases with increasing amplitudes for amplitudes much smaller than the plasma thermal energy per charge (small-amplitude holes) [*Schamel*, 1979, 1986], and that the minimum allowed width increases with increasing potential amplitudes [*Chen*, 2002], and depends on the unperturbed distribution function for small amplitude holes [*Krasovsky et al.*, 1997, 2003].

[3] *Lynov et al.* [1979] performed the first laboratory experiment on electron holes. Their measurements seemed to support the result that the width increases with increasing amplitudes [*Turikov*, 1984] but were not able to address the width-amplitude relation in the small-amplitude limit due to the very limited range of amplitudes that were realized. The first space experiment that addressed the width-amplitude relation was reported by *Ergun et al.* [1998]. They showed that the width increases with increasing potential amplitudes in a range of 0.05–0.7 plasma thermal energy per charge for solitary positive potential structures. *Ergun et al.* [1998] concluded that the observed structures are electron holes. This conclusion was based on the prediction that the width of one-dimensional (1-D) electron holes increases with increasing amplitudes [*Muschietti et al.*, 1999a, 1999b]. The behavior of increasing widths for increasing potential amplitudes was found to also occur for large-amplitude rarefactive ion and electron acoustic solitons [*Ghosh and Lakhina*, 2004a, 2004b].

0148-0227/05/2005JA011087$09.00

[4] *Krasovsky et al.* [2003] derived a minimum allowed width for small-amplitude 1-D electron holes. The minimum allowed width they obtained increases with increasing potential amplitudes and decreases with increasing phase-space density of unperturbed electrons that move at the electron hole velocity (called "the distribution function in resonance"). The explicit dependence on the distribution function is due to that the authors did not solve the coupled Vlasov-Poisson equations exactly but resorted to an approximate approach. The derived restriction on the distribution function and potential amplitudes and widths was compared with solitary waves observed by the Geotail spacecraft [*Kojima et al.*, 1999] to show that the observed solitary waves satisfy the restriction at a rather low value of the distribution function in resonance. The Geotail waveform instrument cannot determine the wave velocity. It was assumed that the solitary potentials are positive and that they travel at the same velocity as the electron beams measured by the plasma instrument on Geotail [*Kojima et al.*, 1999]. The comparison between the Geotail observation and *Krasovsky et al.*'s [2003] theory provides a good hint that electron holes may not follow one-to-one width-amplitude relation, in contrast to the finding based on the FAST observation [*Ergun et al.*, 1998; *Muschietti et al.*, 1999a, 1999b]. However, the incapability of Geotail to experimentally determine whether the observed solitary waves are electron holes and their propagation velocities, along with the limitations on the theory by *Krasovsky et al.* [2003], prevents any conclusive statement to be made on the width-amplitude relation of naturally occurred electron holes.

[5] Theories on 3-D electron holes without ion dynamics [*Chen and Parks*, 2002a, 2002b] and with ion dynamics [*Chen et al.*, 2004] and on ion holes [*Chen et al.*, 2004] have obtained sets of inequalities that constrain the potential amplitude and the widths parallel and perpendicular to the background magnetic field. It has been pointed out that the most distinguished feature of electron and ion holes is that their potential widths do not have to increase or decrease with increasing amplitudes but rather can take any continuous values above a bound that increases with increasing amplitudes and can be of sub-Debye scale [*Chen et al.*, 2004]. The ubiquity of electron holes and ion holes was attributed to this continuum of allowed parameter space. This feature distinguishes phase-space-hole solitary waves from all other known solitons, as the widths and amplitudes of other solitons are of 1-1 mapping relation [*Drazin*, 1983]. Experimental evidence for electron holes whose widths and amplitudes reside in the allowed region but not on the bounding curve or bounding surface has been lacking until the work by *Franz et al.* [2005]. This, in part, is due to the absence of knowledge on how the bounding curves would vary with experimental parameters such as the electron hole velocity, the ion and electron temperatures, and the perpendicular size of electron holes. In this paper, quantitative analysis on the modification of the bounding curve due to various effects will be presented.

[6] The organization of the rest of this paper is as follows. In section 2, we discuss the theoretical origin of the width-amplitude inequality of 1-D electron holes and derive a coarse but unbreakable bound that is independent of ambient plasma distributions and solitary potential forms. Next, we obtain an exact width-amplitude inequality for 1-D electron holes neglecting ion dynamics and finite hole velocities in section 3. We then show in section 4 how the inequality is modified separately by the inclusion of ion dynamics and effects of finite perpendicular size (3-D). Section 5 presents the results for finite hole velocities, while section 6 illustrates the signatures in distribution functions of electron holes. In section 7, we demonstrate that the observed 3-D electron holes reported in the work of *Franz et al.* [2005] populate an allowed region significantly away from the bounding curve and thus represent a strong evidence for the accessibility of loosely constrained electron holes. We discuss the impact of the existence of loosely constrained electron holes in section 8. Finally, we summarize and conclude in section 9.

2. Origin of Width-Amplitude Inequality

[7] Electron phase space holes are localized potential humps that are self-consistently sustained by electrons bouncing back and forth inside the potential energy trough and by electrons and ions streaming into and out of the potential structure in a collisionless plasma. The lack of binary collisions preserves the total energy of each particle and prevents the mixing of electrons that are trapped (bouncing inside the potential) and those that are passing (streaming into and out of the potential). The potential hump originates exclusively from the collective electric field of all electrons and ions, and this collective field in turn determines how electrons and ions are distributed in phase space. This coupling between the mean field of the plasma particles and the distribution functions is described by the nonlinear Vlasov-Poisson equations.

[8] Electron and ion phase space holes are solitary wave solutions of the nonlinear Vlasov-Poisson equations that involve trapping of only electrons and ions, respectively. They are also called Bernstein-Greene-Kruskal (BGK) solitary waves [*Bernstein et al.*, 1957], as Bernstein, Greene, and Kruskal were the first to obtain the exact, time-stationary solutions for the 1-D nonlinear Vlasov-Possion equations. In the original BGK work, it is recognized that in theory collisionless plasmas can support quite arbitrary potential forms in one dimension by distributing plasma particles that are trapped inside the potential energy troughs. The only constraint is that the number of trapped particles in any differential phase space volume cannot assume negative values ($f_{tr} \geq 0$). As the authors remarked themselves, whether these waves can be found in reality depends on factors that are not considered in their paper which include the accessibility and stability of the waves. Because the BGK work provides only general solutions, it was not clear how arbitrary the potential forms can be and how the constraint on the trapped particle distribution should translate to a constraint on macroscopic variables such as the potential width and amplitude.

[9] We can obtain an intuitive understanding for why there exists a width-amplitude inequality for electron holes based on the following simple consideration. When there is a solitary potential hump, the responses of passing electrons and ions are known. Electrons from outside the potential hump would speed up and then slow down as they pass through the hump. Ions would either be reflected if their total energy is not sufficient to overcome the potential

energy barrier or slow down and then speed back up as they pass through the hump. As the velocity profiles of passing electrons and ions are known, their density profiles are known. The question is whether one can find a way to distribute electrons inside the potential hump (or potential energy trough) so that the hump is completely sustained by the plasma itself. In mathematical terms with dimensionless units, we observe the following:

$$\rho = -n_{tr} - n_p + n_i$$
$$n_{tr} = -\rho - n_p + n_i \geq 0, \tag{1}$$

where ρ is the dimensionless total charge density due to the localized potential hump, n_{tr} is the number density of electrons trapped inside the potential hump, n_p is the density of passing electrons, and n_i is the ion density. No number densities can take negative values, thus one must have $n_{tr} \geq 0$. Where the potential is zero (ρ is zero), we normalize the unperturbed densities $n_p = n_i = 1$.

[10] The most severe constraint in equation (1) occurs where ρ is the most positive, which occurs at the peak of the potential hump. By the Poisson equation ($\rho = -\partial^2\phi/\partial x^2$), Max($\rho$) scales as ψ/δ^2, where ψ is the peak amplitude and δ the spatial width of the potential. For simplicity, we neglect ion dynamics and only note that n_i would become less than 1 inside the potential (this would become evident in later treatment where ion dynamics is included) and hence ion dynamics would not change the qualitative nature of the width-amplitude relation. The last part of the above inequality hence becomes

$$\mathrm{Max}(\rho) \sim \psi/\delta^2 \leq n_i - n_p \leq 1 - n_p < 1 \longrightarrow \delta > \sqrt{\psi},$$

where we have used the important fact that the passing electron density within the potential is always less than its ambient value (unity) as their velocities are always larger than the ambient values. We thus see from the above how the requirement of a nonnegative trapped electron density everywhere inside the potential translates to an inequality between the potential width and amplitude. Note that in the above argument, specific forms of the potential and the passing electron and ion distribution functions are not given. Therefore the fact that the width and amplitude of electron holes are constrained by an inequality is independent of specific potential and distribution functions. The above simple consideration gives us a coarse bound on the allowed potential amplitude and width: the width has to be greater than $\sqrt{\psi}$. This bound on the minimum allowed width increases with potential amplitude ψ.

[11] It is important to note the underlying reason for the distinction between the width-amplitude relations for phase-space hole solitary waves and fluid solitons. Fluid solitons in a plasma, such as acoustic solitons, are based on nonlinear equations of fluid quantities which involve further reduction of degrees of freedom from the Vlasov-Poisson description, that is, integrating distribution functions to obtain fluid moments. For phase space holes, there is no such reduction of degrees of freedom, and therefore they are more general forms of solitary structures in a collisionless plasma than fluid solitons. The reduction of degrees of freedom results in the strict 1-1 mapping relation between the spatial size and potential amplitude of fluid solitons. Furthermore, fluid solitons can only assume scale sizes in fluid scales. For example, their sizes have to be larger than the Debye length which is the characteristic scale length for local equilibrium [*Debye and Hückel*, 1923; *Jackson*, 1990] and the smallest length at which the plasma can behave like a fluid [*Bohm and Gross*, 1949]. On the other hand, phase-space holes are intrinsically nonlinear and nonequilibrium. Their existence relies on the lack of efficient mechanisms to equilibrium, namely, lack of effective binary collisions. The screening of the positive charge core of a 1-D electron hole is accomplished exclusively by electrons trapped inside the potential structure, and not by thermal (Debye) screening [*Chen and Parks*, 2002b; *Chen et al.*, 2004]. The size of electron holes therefore is not restricted to be larger than the Debye length, insofar as the Vlasov-Poisson equations are still applicable. In a plasma with λ_D = 500 m and a density 0.5 cm^{-3}, (typical for the polar plasma sheet boundary, the region where events in Figure 10 were taken), there are of order $\sim 10^6$ particles in a phase-space hole solitary wave of width $\sim 0.01\ \lambda_D$. This is well within the applicability of the Vlasov description.

[12] The existence of width-amplitude inequalities for phase space holes depends crucially on the dimensionality of the velocity space. It has been analytically shown that for an isotropic unmagnetized plasma, if the velocity space is two- or three-dimensional, there do not exist fully localized time-stationary solutions to the nonlinear Vlasov-Poisson equations [*Chen*, 2002]. The reason is that in 2-D and 3-D unmagnetized plasmas, the passing particle density does not decrease with the potential amplitude, and the plasma cannot self-consistently support the charge core according to the Poisson equation. The lack of BGK solutions was thought to be the reason for the short lifetime of 2-D and 3-D electron holes in zero magnetic fields observed in simulations performed by *Morse and Nielson* [1969]. Similar discussions from a different perspective can be found in the work of *Krasovsky et al.* [2004]. Exact 3-D electron hole solutions were constructed in three spatial dimensions, while keeping the velocity space one-dimensional, that is, for 3-D magnetized plasmas with negligible cyclotron radius [*Chen et al.*, 2004]. A more in-depth analysis on the effects of velocity space dimensionality will be published elsewhere [*Chen et al.*, 2005].

3. One-Dimensional Width-Amplitude Inequality: No Ion Dynamics and Zero Hole Velocity

[13] In this section, we discuss characteristics of the width-amplitude relation for 1-D electron holes that have zero velocity in the ambient plasma frame. Ion dynamics is ignored. Such a solution for the trapped electron distribution function has been obtained by *Chen and Parks* [2002b] for a Gaussian solitary potential

$$\phi(\psi, \delta, x) = \psi e^{-x^2/2\delta^2}, \tag{2}$$

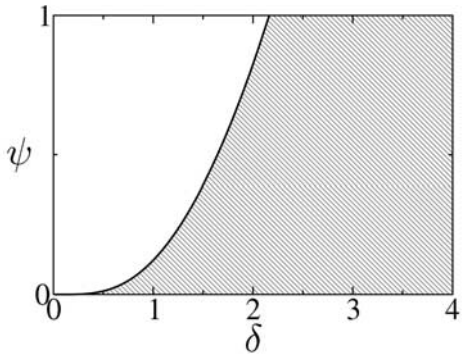

Figure 1. The width-amplitude relation for one-dimensional (1-D) electron holes with zero hole velocity and no ion dynamics. The curve and shaded region mark the allowed widths and amplitudes for the plotted range. The amplitude is normalized by the electron thermal energy per charge, and the width by the electron Debye length.

and Maxwellian distributed ambient electron distribution whose density outside the solitary potential has been normalized to 1 (the background ion density),

$$f_p(w) = \frac{\sqrt{2m_e}}{\sqrt{\pi T_e}} e^{-w/T_e}, \tag{3}$$

where $w = m_e v^2/2 - e\phi$. Note that in order to be formally consistent with the following sections when ion dynamics (and thus ion mass) is present, we have put back the dimensions here as opposed to the dimensionless forms in the work of *Chen and Parks* [2002b]. In this and the following sections, whenever dimensionless quantities are presented, the energy unit is taken to be the ambient electron thermal energy T_e, the length unit is the ambient electron Debye length $\lambda_D = \sqrt{T_e/4\pi ne^2}$, the charge unit is the unsigned electron charge e, and the velocity is the ambient electron thermal velocity. Here, we reproduce the trapped electron distribution (apart from an overall coefficient involving the mass) from *Chen and Parks* [2002b] as follows in order to obtain the width-amplitude relation

$$\frac{f_{tr}(\psi,\delta,w)}{\sqrt{2m_e}} = \frac{2\sqrt{-w}}{\pi\delta^2}\left[1 - 2\ln\left(\frac{-4w}{\psi}\right)\right] + \frac{e^{-w}}{\sqrt{\pi}}\left[1 - \mathrm{erf}\left(\sqrt{-w}\right)\right]. \tag{4}$$

[14] As discussed by *Chen and Parks* [2002b], the global minimum of the above f_{tr} occurs at $w = -\psi$, that is, the trapped electron phase space density takes its minimum for the electrons that are at rest at the peak of the potential hump. Hence the condition $f_{tr}(w = -\psi) \geq 0$ guarantees a physical trapped electron distribution and results in the width-amplitude inequality

$$\delta \geq \left[\frac{2\sqrt{\psi}(4\ln 2 - 1)}{\sqrt{\pi}e^{\psi}[1 - \mathrm{erf}(\sqrt{\psi})]}\right]^{1/2}. \tag{5}$$

We plot equation (5) for a range of allowed amplitudes and widths in Figure 1. A point in the shaded region represents an allowed electron hole with a given ψ and δ. The shaded region includes all of the allowed ψ and δ for the range of values shown. For a fixed δ, all $\psi \leq \psi_0$ are allowed, where ψ_0 is such that $f_{tr}(\psi_0, \delta, w = -\psi_0) = 0$; while for a fixed ψ, all $\delta \geq \delta_0$ are allowed, where δ_0 is such that $f_{tr}(\psi, \delta_0, w = -\psi) = 0$. From equation (5) we know that for 1-D electron holes, at the level of no ion dynamics and zero hole velocity, there are no absolute upper or lower bounds on the potential amplitude and the width within the Vlasov-Poisson theory. The Debye length is not a characteristic length for electron holes. In fact, it does not even come into the formulation. We only use it as a unit for lengths, analogous to the usage of a centimeter as a length unit while a centimeter is by no means characteristic to the object being measured.

[15] In the large-amplitude limit $\psi \gg 1$, the widths and amplitudes are constrained by $\delta \geq \sqrt{\psi}$ which coincides with the coarse bound found in the previous section. In the small-amplitude limit $\psi \ll 1$, the constraint is $\delta \geq \psi^{1/4}$. This exact bound obtained from solving for the trapped distribution is only slightly tighter than the coarse bound. This comparison with the coarse bound tells us how general the width-amplitude inequality is; different functional forms of the potential hump and passing electron distribution do not alter the bounding curve much. For example, solitary potentials of the form $\psi\,\mathrm{sech}\,(x/\delta)^n$, where n is a positive even integer, yield the same width-amplitude constraints in both the small- and large-amplitude limits [*Turikov*, 1984]. The equal sign in equation (5) corresponds to the case of empty-centered electron holes studied by *Turikov* [1984]. Figure 1 can be compared directly to the figure in the work of *Muschietti et al.* [1999b] to see that our bounding curve is quantitatively similar to their width-amplitude curve which was obtained using a flat-topped passing electron distribution [*Muschietti et al.*, 1999a] and that the electron holes observed by FAST lie closely on the bounding curve within error bars.

[16] We note that the bounding curve given by taking only the equal sign in equation (5) corresponds to electron holes with zero phase-space density at the hole center and is where the largest electric field amplitudes occur. For a given potential amplitude, the point on the bounding curve yields the smallest allowed width, while for a given width, it gives the largest allowed potential amplitude. In both cases, the point on the bounding curve gives the largest electric field amplitude. In simple terms, the farther away an electron hole is from the bounding curve, the smaller electric field amplitude it has. Therefore to uncover electron holes that dwell deep inside the allowed width-amplitude space, it is critical to resolve small-amplitude electric fields. The FAST observation of electron holes clustering only on the bounding curve [*Ergun et al.*, 1998, 1999; *Muschietti et al.*, 1999a] is likely due to their emphasis on events with large electric field amplitudes ($\geq$50 mV/m).

4. Effects of Ion Dynamics and Finite Perpendicular Size

[17] In the context of 3-D electron holes, the width-amplitude relation has been obtained by *Chen et al.* [2004] incorporating ion dynamics for azimuthally symmetric double Gaussian potentials,

$$\Phi(r,z) = \psi\,\exp\left(-z^2/2\delta_z^2 - r^2/2\delta_r^2\right), \tag{6}$$

and Boltzmann-type isotropic ambient electron and ion distributions,

$$f_p(w) = \sqrt{2m_e/\pi T_e}\exp(-w/T_e), \tag{7}$$

$$f_i(w) = \sqrt{2m_i/\pi T_i}\exp(-w/T_i), \tag{8}$$

where $w = m_{e,i}v^2/2 + q_{e,i}\Phi(r, z)$. Here we outline their key expressions for the trapped electron density n_{tr}, trapped electron distribution f_{tr}, and the width-amplitude relation, in order to discuss separately effects of ion dynamics and finite perpendicular size. To make clear how the ion parameters T_i, q_i, and m_i may come into later calculations, we have deliberately written out the dimensional forms for f_p and f_i. The dimensionless trapped electron density as a function of the potential (and hence the cylindrical coordinates r and z) was obtained to be

$$n_{tr}(\Phi) = \Phi\left[\frac{r^2}{\delta_r^2}\left(\frac{1}{\delta_r^2}-\frac{1}{\delta_z^2}\right)-\frac{2}{\delta_r^2}-\frac{1}{\delta_z^2}-\frac{2}{\delta_z^2}\ln\left(\frac{\Phi}{\psi}\right)\right] - e^{-\Phi}\left[1-\mathrm{erf}\left(\sqrt{-\Phi}\right)\right]+\exp\left(-t\Phi\right), \tag{9}$$

where δ_z and δ_r are the parallel and perpendicular widths of the potential, $t \equiv q_iT_e/T_i$ is the product of the electron to ion thermal energy ratio and the unsigned ion to electron charge ratio (written as q_i as charge is in unit q_e). The above expression for n_{tr} corresponds term by term to equation (1) with the first term on the right-hand side $-\rho$, the second term $-n_p$, and the third term n_i. Here we see that $n_i = \exp(-t\Phi)$ is always less than unity when Φ is positive.

[18] The trapped electron distribution obtained by *Chen et al.* [2004] reads

$$\frac{f_{tr}(r,w)}{\sqrt{2m_e}} = \frac{2\sqrt{-w}}{\pi}\left[\frac{r^2}{\delta_r^2}\left(\frac{1}{\delta_r^2}-\frac{1}{\delta_z^2}\right)-\frac{2}{\delta_r^2}+\frac{1}{\delta_z^2}-\frac{2}{\delta_z^2}\ln\frac{4w}{-\psi}\right] + \frac{e^{-w}}{\sqrt{\pi}}\left[1-\mathrm{erf}\left(\sqrt{-w}\right)\right]-\frac{e^{tw}}{\sqrt{\pi}}\sqrt{t}\ \mathrm{erfi}\left(\sqrt{-tw}\right), \tag{10}$$

and the width-amplitude relation

$$\delta_z \geq \sqrt{\frac{2\sqrt{\psi}(4\ln 2-1)}{F_p(\psi,t)-4\sqrt{\psi}/\delta_r^2}}, \tag{11}$$

where

$$\frac{F_p(\psi,t)}{\sqrt{\pi}} = e^{\psi}\left[1-\mathrm{erf}\left(\sqrt{\psi}\right)\right]-e^{-t\psi}\sqrt{t}\ \mathrm{erfi}\left(\sqrt{t\psi}\right).$$

Note that the trapped distribution has a mass factor associated with it. For electron holes, the expression on the right-hand side of equation (10) is the trapped electron distribution divided by $\sqrt{2m_e}$, while for ion holes, the same expression with $t \equiv T_i/q_iT_e$ is the trapped ion distribution divided by $\sqrt{2m_i}$. In the above expression for F_p, the first term on the right-hand side comes from passing electrons, and it is the same as the passing electron contribution in equation (5). The second term involves t and is from the ion contribution. The complex error function defined as $\mathrm{erfi}(z) = \mathrm{erf}(iz)/i$ is a real function of its argument. The limit of $t = 0$ sets the entire term involving t to zero and corresponds to the limit of no ion dynamics. This limit is justified as when ions are very hot ($T_i \to \infty$), the motion of most ions is not altered by the potential hump, and thus their density perturbation is negligible. On the other hand, the limit of $\delta_r \to \infty$ recovers the 1-D solutions. Setting both $t = 0$ and $\delta_r \to \infty$ reduces equation (11) to equation (5). By comparing equations (5) and (11), we see mathematically how the ion dynamics and finite perpendicular size come in to modify the relation between the allowed potential amplitude and parallel width.

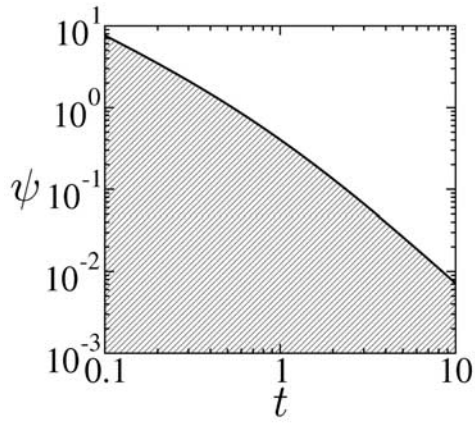

Figure 2. The allowed potential amplitudes of 1-D electron holes (infinite perpendicular size) as a function of $t = q_iT_e/T_i$, where q_i is the ion charge in units of the electron charge. The larger t (the larger the electron to ion temperature ratio, and thus the more involved the ion dynamics), the smaller the potential amplitude of electron holes is allowed to get up to. In the limit of $t = 0$ (no ion dynamics), the amplitude does not have an upper bound.

[19] We need to develop further how the participation of ions and multidimensionality (finite perpendicular size) modifies the allowed parameter space before we demonstrate their separate effects. In addition to the constraint presented in equation (11), since the denominator in equation (11) has to be positive definite, more constraints arise

$$F_p(\psi,t) > 0; \tag{12}$$

$$\delta_r^2 > 4\sqrt{\psi}/F_p(\psi,t). \tag{13}$$

Equation (12) is plotted in Figure 2 to show that when ion dynamics is included, there exists a maximum allowed potential amplitude for a given t, the electron to proton temperature ratio, if an electron-proton plasma is assumed. The smaller the electron to ion temperature ratio, the larger the bound on the allowed potential amplitude. If the ions are in a higher charged state (larger q_i), say O^{2+}, then the same temperature ratio would give rise to a t that is twice as large and results in a tighter bound on the allowed potential amplitude. It is interesting to note that for ion phase-space holes, a higher charged state would result in a looser bound given the same temperature ratio [*Chen et al.*, 2004].

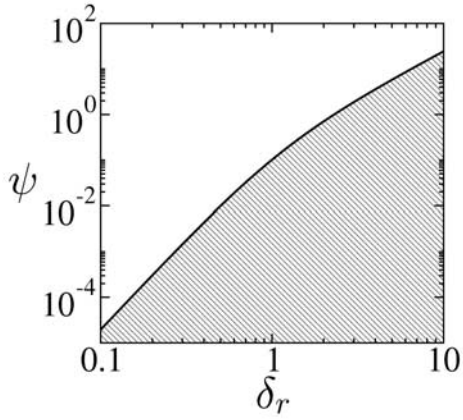

Figure 3. The allowed potential amplitude as a function of the perpendicular size (δ_r) of electron holes neglecting ion dynamics. The larger δ_r, the larger the maximum allowed amplitude. In the limit of $\delta_r \to \infty$, the amplitude has no upper bound.

[20] Setting $t = 0$ in equation (13), we obtain the constraint on the maximum allowed potential amplitude due to the finite perpendicular size, and we plot the resulting inequality in Figure 3. For each value of the perpendicular size, there is an upper bound on the allowed potential amplitude. The smaller the perpendicular size, the tighter the bound. From Figures 2 and 3, we see that both ion dynamics and the perpendicular size impose an upper bound on the potential amplitude which does not exist in Figure 1 where effects of ion dynamics and finite perpendicular size are not included.

[21] We are now ready to see how the parallel width and amplitude relation is modified separately by the inclusion of ion dynamics and the finite perpendicular size. We set $\delta_r \to \infty$ in equation (11) and plot the remaining inequality in Figure 4 for t = 0,0.1,1,10. Points on and below the bounding curves are allowed. The larger t (the larger electron to ion temperature ratio), the more important the ion dynamics, and that results in tighter allowed parameter space. The bounding curves for $t = 1$ and 10 are flat above

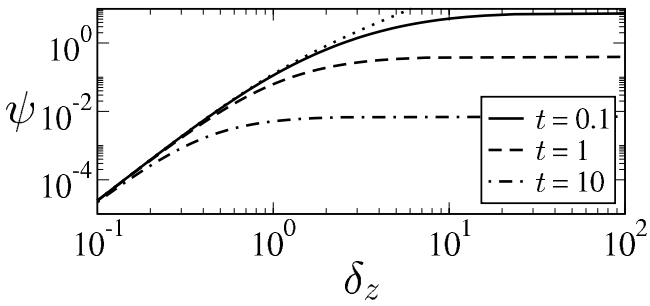

Figure 4. The bounding curves for allowed widths and amplitudes of 1-D electron holes for different values of $t = q_i T_e / T_i$. Points on and below each curve are allowed for the corresponding t. The dotted curve is for $t = 0$, that is, no ion dynamics. The larger t (the colder ions with respect to electrons, and thus the more important ion dynamics), the smaller the allowed width-amplitude space. Note the cutoff amplitudes for nonzero t.

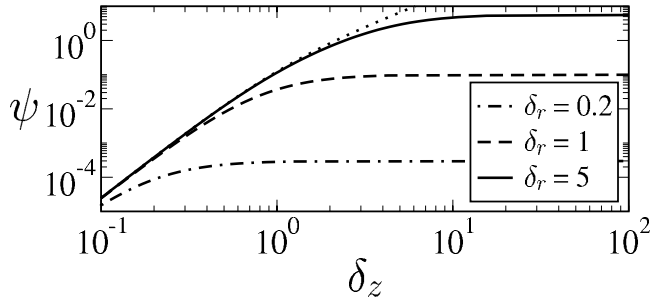

Figure 5. The bounding curves for allowed parallel widths and amplitudes of 3-D electron holes neglecting ion dynamics for different perpendicular size (δ_r). Points on and below each curve are allowed for the corresponding δ_r. The dotted curve is the asymptotic bounding curve for $\delta_r \to \infty$. Not only does the allowed width-amplitude space shrink for decreasing δ_r but there is a cutoff in allowed amplitude for a given finite δ_r.

certain widths, exhibiting the upper bounds on potential amplitudes discussed earlier due to finite temperature ratios. To see the effect of finite perpendicular size (δ_r), we set $t = 0$ in equation (11) and plot the inequality in Figure 5 for δ_r = 0.2, 1,10 and ∞. Points on and below each curve represent allowed widths and amplitudes for each corresponding δ_r. One can see that the allowed space shrinks for decreasing perpendicular size. The flattening of the bounding curves is a result of the upper bounds on potential amplitudes due to finite perpendicular size (as shown in Figure 5).

[22] Combining effects of ion dynamics and finite perpendicular size, we plot equation (11) for two t values in Figure 6. Points on and above the bounding surface A are

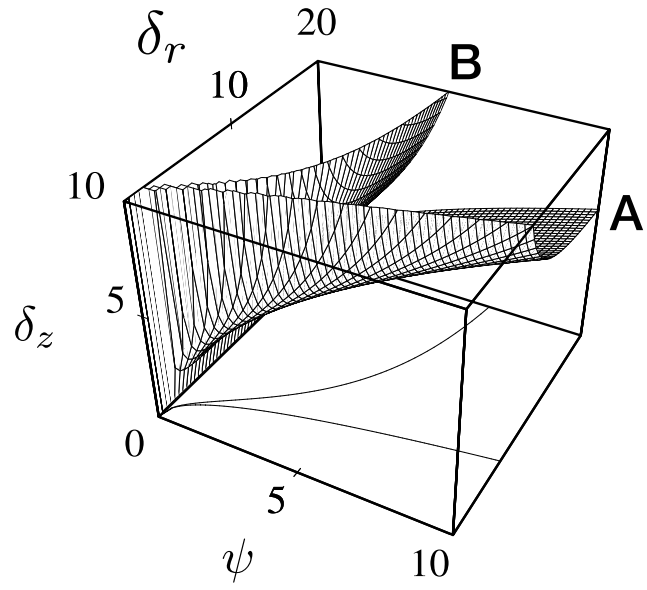

Figure 6. The relation between the potential amplitude ψ, the parallel width (δ_z) and the perpendicular width (δ_r) for 3-D electron holes. Points on and above surface A are allowed amplitudes and widths when ion dynamics is not considered ($t = q_i T_e / T_i = 0$), and on and above surface B is the allowed space for $t = 0.1$ The colder ions are relative to electrons, the more important the ion dynamics, and the tighter the allowed parameter space.

allowed parameters (ψ, δ_z, δ_r), for $t = 0$ (no ion dynamics), and points on and above surface B are allowed for $t = 0.1$. The allowed space for ψ and δ_z shrinks when ion dynamics is more important (larger t) and when the perpendicular size (δ_r) is smaller.

5. Effects of Finite Hole Velocity

[23] In this section, we demonstrate how finite electron hole velocity normalized by the ambient electron thermal velocity (called the Mach number) modifies the inequality between the potential amplitude and parallel width. To single out this effect, we do not include ion dynamics and finite perpendicular size in this section. *Turikov* [1984] has obtained the equality width-amplitude relation for 1-D electron holes for different Mach numbers neglecting ion dynamics. His result is that for a fixed potential amplitude the width increases with increasing Mach number, and for a fixed width the potential amplitude decreases with increasing Mach number. His result was obtained numerically, as for a Maxwellian passing electron distribution there exists no analytical expression for the trapped electron distribution with nonzero Mach number.

[24] To demonstrate the Mach number effect in a simple and clean way, we first use a Lorentzian passing electron distribution (also called the Cauchy distribution; see *Gurnett and Bhattacharjee* [2005] for more information about the distribution) which allows an analytical trapped electron distribution with nonzero Mach number. The passing electron distribution reads

$$f_p(w) = \sqrt{\frac{m_e}{\pi}}\left(\frac{1}{\left(\sqrt{w}-M\right)^2+1}+\frac{1}{\left(\sqrt{w}+M\right)^2+1}\right), \quad (14)$$

where M is the Mach number, and the normalization constant is chosen such that the unperturbed passing electron density is 1. Again the mass factor is retained for consistency with previous sections. The trapped electron distribution function is then obtained as

$$\frac{f_{tr}(w)}{\sqrt{2m_e}} = \frac{2\sqrt{-w}}{\pi\delta^2}\left[1-2\ln\left(\frac{-4w}{\psi}\right)\right]+\frac{\left(\sqrt{-w}+1\right)}{\sqrt{\pi}\left(\left(\sqrt{-w}+1\right)^2+M^2\right)}. \quad (15)$$

Comparing equation (15) to equation (4), we can see that the first term from the solitary potential is unchanged. It is only the second term in f_{tr} coming from the passing electrons that is different, and this term is positive definite and monotonically decreasing from $w = 0$ to $w = -\psi$ for any given Mach number. The width-amplitude relation for this case is obtained by the condition $f_{tr}(w = -\psi) \geq 0$ to be

$$\delta \geq \left[\frac{\sqrt{\psi}(4\ln 2-1)\left(M^2+\left(\sqrt{\psi}+1\right)^2\right)}{2\left(\sqrt{\psi}+1\right)}\right]^{1/2}. \quad (16)$$

From equation (16), we can see immediately that the right-hand side would increase with increasing M, which means that the lower bound of the width would become larger for larger M, hence the allowed space would shrink. From the manner M appears in equation (16), we also see that when $M \ll 1$, the effect of finite Mach number on the width-amplitude relation is small, and approaches zero as $M \to 0$.

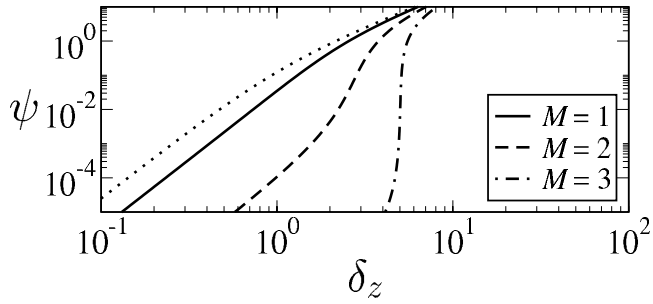

Figure 7. Allowed width-amplitude space of 1-D electron holes neglecting ion dynamics for Mach number (hole velocity normalized by the electron thermal velocity in the ambient electron frame) $M = 0,1,2,3$. Points on and to the right of the bounding curves are allowed. Increasing M shrinks the allowed space.

[25] Now that we have seen analytically how the Mach number influences the allowed parameter space, we illustrate this influence for a Maxwellian passing electron distribution in Figure 7 for quantitative comparison with our results in other sections where a Maxwellian ambient electron distribution is used. The bounding curves are obtained numerically. Our result is that increasing Mach number shrinks the allowed parameter space but in a way different from those by the inclusion of ion dynamics and finite perpendicular size. In particular, for small-amplitude electron holes ($e\phi/T_e \leq 10^{-2}$), the minimum allowed potential width is raised significantly when the Mach number M goes up to 2 and 3. For $M \geq 2$, the minimum allowed width cannot be smaller than one Debye length unless the potential amplitude becomes extremely small ($\psi < 10^{-4}\ T_e/e$). High Mach number ($M \geq 2$) electron holes therefore may be hard to detect even if they exist. This may account for the fact that the observed electron holes all have Mach numbers less than 2 [*Franz*, 2000; *Franz et al.*, 2005].

6. Signatures in Distribution Functions

[26] It is worthwhile to illustrate the different signatures of electron velocity distributions for solutions that dwell on the bounding curve and those that do not. So far, the capabilities of laboratory and space experiments cannot resolve the phase space structures of electron holes. As experimental techniques advance, the phase space structure of a single electron hole may be resolved in the future. We provide in this section examples of electron distributions for future comparison with experiments. In Figure 8, we plot the normalized distribution function that represents $\sqrt{\pi T_e/2m_e}f_{tr}$ (thick curves) and $\sqrt{\pi T_e/2m_e}f_p$ (thin curves) at $r = 0$ and $z = 0$ as a function of velocity v (T_e is numerically 1 as it is the energy unit and is kept explicitly for clarity in dimensions). The distribution functions here are the f_p and f_{tr} in section 4. The solid curves in both Figures 8a and 8b correspond to an electron hole that has zero phase space density at its phase space center ($r = 0$, $z = 0$, $v = 0$). When the size of the structure is fixed, decreasing the amplitude raises the center phase space density as shown

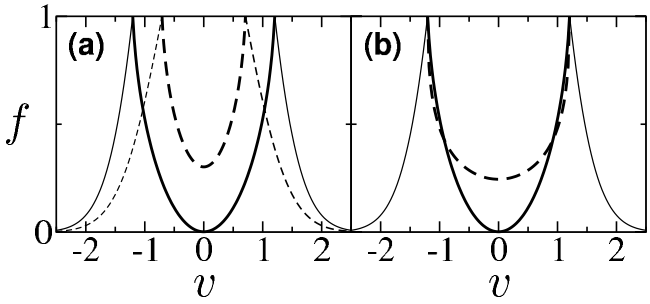

Figure 8. Normalized electron velocity distributions at the center ($r = 0$, $z = 0$) of electron holes for different potential amplitudes (ψ) and parallel sizes (δ_z): (a) (ψ, δ_r, δ_z) = (1.45, 5, 3) (solid lines) and (ψ, δ_r, δ_z) = (0.5, 5, 3) (dashed lines), (b) (ψ, δ_r, δ_z) = (1.45, 5, 3) (solid lines) and (ψ, δ_r, δ_z) = (1.45, 5, 10) (dashed lines). In both cases the thick lines represent trapped electron distributions for the specified parameters, and the thin lines are passing electron distributions. With the same size, decreasing the potential amplitude raises the phase space density of trapped electrons, and the separatrices between trapped and passing electrons are squeezed inward to lower velocities. With the same amplitude and perpendicular size (δ_r), increasing the parallel size raises the phase space density of trapped electrons but leaving the separatrices at the same velocities. The effect of varying the perpendicular size is similar to varying the parallel size (not shown).

by the dashed curve in Figure 8a. On the other hand, increasing the amplitude would lower the center phase space density from zero to a negative value (not shown) and hence result in unphysical solutions. When the amplitude is fixed, increasing the parallel size raises the center phase space density as shown in Figure 8b by the dashed curve. Varying δ_r results in a similar effect.

[27] In summary, electron holes whose widths and amplitudes follow the equal sign in the width-amplitude relation have zero phase space density at the center of their phase space structure, and those that do not follow the equal sign have finite phase space density at the center. The simulation study on 1-D electron holes by *Omura et al.* [1996] has shown formation of electron holes with finite phase-space density at the hole center for a bump-on-tail unstable initial condition [*Omura et al.*, 1996, Figure 7]. The studies by *Turikov* [1984] and *Muschietti et al.* [1999a, 1999b, 1999c] drew conclusions about how the width should vary with potential amplitudes only from a subset of solutions, the empty-centered electron holes, and hence they concluded that the width must increase for increasing amplitudes despite that formally a 1-D width-amplitude inequality was obtained by *Muschietti et al.* [1999a]. On the other hand, the conclusion that the width decreases with increasing amplitudes by *Schamel* [1979] was due to a different subset of allowed solutions that assume finite values at the centers of the phase space holes.

7. Comparison With Space Observations

[28] Having discussed the origin and characteristics of the width-amplitude inequality and how the inequality is quantitatively modified by the effects of ion dynamics, finite perpendicular size, and hole velocity in previous sections, we now compare our theoretical predictions with the electron holes observed by the Polar Plasma Wave Instrument (PWI) [*Gurnett et al.*, 1995]. The detailed observational properties of these electron holes are presented by *Franz et al.* [2005]. In this section we focus only on how the observed electron holes populate the allowed parameter space. Plotted in Figure 9 as dots are the parallel widths and potential amplitudes of 2067 electron hole events measured in the polar cusp. The solid curve is the theoretical bounding curve for $M = 0.3$, $\delta_r = 2$, and $T_e/T_i = 0.1$. The temperature ratio is taken from the Hydra electron and ion data. The perpendicular size is not directly measured, but as inferred by *Franz et al.* [2005], most of the structures have their perpendicular widths larger than parallel widths which are predominantly greater than 1 (λ_D). Therefore we use $\delta_r = 2$ to draw the bounding curve as we have learned from section 4 that wider perpendicular size would yield a looser bound. We would like to compare the data with the tightest bound for relevant conditions in order to show that there are significant amounts of electron holes residing deep in the allowed region. The Mach number is taken to be 0.3, since the most probable Mach number is reported to be 0.3 for the cusp events [*Franz et al.*, 2005]. Most of the observed Mach numbers are less than 1 [see *Franz et al.*, 2005, Figure 9], and the location of the bounding curve does not vary much for Mach number 0.3 to 1 according to Figure 7 (the dotted curve is for $M = 0$ and solid curve for $M = 1$); therefore the bounding curve for $M = 0.3$ presents well the Mach number effect. Almost all the data points are in the allowed region, and they cover a wide range of $\sim$3 orders of magnitude in widths as well as in amplitudes. Most of the events cluster in the region with widths 1–10 Debye lengths and amplitudes 10^{-4}–10^{-2} electron thermal energy per charge. This region is significantly away from the bounding curve. These electron holes therefore are evidence for the accessibility of allowed solutions far away from the bounding curve.

[29] Previous space [*Ergun et al.*, 1998, 1999; *Cattell et al.*, 2003] and laboratory [*Lynov et al.*, 1979] measurements of electron holes are consistent with the results of widths

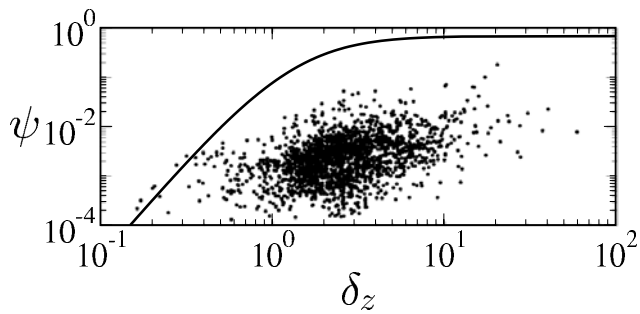

Figure 9. The potential amplitudes and parallel widths of 3-D electron holes observed by Polar Plasma Wave Instrument (PWI) compared with the theoretical bounding curve for $M = 0.3$, $T_e/T_i = 0.1$, and $\delta_r = 2$. A large fraction of data points lie significantly away from the bounding curve, presenting the evidence that Nature can realize electron holes that dwell not just on the bounding curve but deep into the allowed space. These electron holes were observed in the Polar cusp.

increasing with amplitudes and do not reveal the inequality aspect, probably due to limited dynamical range in observed widths and amplitudes and an emphasis on events with large electric field amplitudes. The only definitive observation-theory comparison on the width-amplitude behavior of electron holes showed that the observed events clustered only on the bounding curve within error bars. There is therefore the question of whether allowed electron holes away from the bounding curve exist in reality. Our electron hole theory although predicting the existence of solutions away from the bounding curve cannot address whether they would be too unstable to be detected nor comment on whether they can be realized in reality. The electron hole observations by Polar PWI, together with our theoretical width-amplitude prediction, directly addressed this previously unresolved issue. As discussed in section 3, electron holes that are farther away from the bounding curve have smaller electric field amplitudes than those that are closer to the bounding curve. We emphasize that the capability of Polar PWI to measure small-amplitude electric fields is critical in uncovering the electron holes that dwell deep in the allowed parameter space, and thus in revealing the inequality aspect of the width-amplitude relation.

[30] In Figure 10, we present another comparison with a different set of 764 electron hole events measured at the plasma sheet/plasma sheet boundary layer (PS/PSBL). In this geospace region, the observed electron holes tend to have smaller size. A significant portion (~65%) of the events are of sub-Debye scale, a feature not possible for fluid solitons but allowed for phase space holes as discussed in section 2. The solid curve is the theoretical bounding curve for $M = 0.1$, $\delta_r = 1$, and $T_e/T_i = 0.5$. A majority of the observed events lie in the allowed region and significantly away from the bounding curve, again demonstrating the accessibility of solutions whose widths and amplitudes are only loosely constrained.

[31] A small fraction of data points that are of very small size ($0.02-0.3\ \lambda_D$) fall outside the allowed region. One possibility is that these electron holes do not pass by the spacecraft along their symmetry axis where the peak potential and the widest parallel width occur. This possibility is supported by the observational feature that the perpendicular electric fields of a series of the PS/PSBL electron holes have the same polarity [*Franz et al.*, 2005, Figure 7], indicating that this group of electron holes pass by the spacecraft at their sides and all at the same side as pointed out by *Franz et al.* [2005]. Note that the ψ and δ_z in our theory (and all other electron hole theories) are the peak potential amplitude and the parallel width along the symmetry axis of the azimuthally symmetric electron holes. Cutting through an electron hole at the side results in sampling a smaller potential amplitude and width and thus may place an electron hole with an allowed width and amplitude in the forbidden region. More generally speaking, this effect would shift the actual amplitudes and widths toward the bounding curve and beyond (lower amplitudes and smaller widths). Since our main goal here is to present evidence for electron holes that are in the allowed region but away from the bounding curve, taking into account this effect would make our point even stronger by shifting some of the data points back into the allowed region and farther away from the bounding curve.

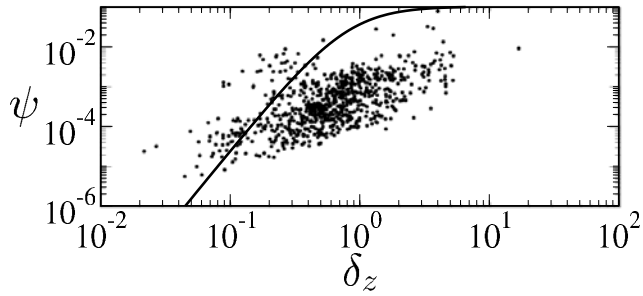

Figure 10. The potential amplitudes and parallel widths of 3-D electron holes observed in the plasma sheet/plasma sheet boundary layer by Polar PWI. The solid curve is the theoretical bounding curve for $M = 0.1$, $T_e/T_i = 0.5$, and $\delta_r = 1$. A large fraction of data points fall under and far away from the bounding curve. The comparison provides the evidence that in this geospace region electron holes that populate well into the allowed width-amplitude space are realizable.

[32] What would happen when the perpendicular motion of the plasma comes into play? In the theory considered above, the perpendicular motion of the plasma is not included, that is, effects of finite gyroradius are ignored. Our solutions describe electron holes for which the gyroradius of electrons (r_g) is much smaller than the size of the solitary structure. When the electron gyroradius is comparable or larger than the structure's parallel and perpendicular size ($r_g \sim \delta_z$, δ_r or $r_g > \delta_z$, δ_r), the electron holes are expected to be less stable and thus have shorter life time [*Muschietti et al.*, 2000, 2002; *Chen et al.*, 2004] but not a tighter allowed width-amplitude space. In fact, the allowed width-amplitude space is expected to be larger for solutions that are valid for r_g comparable to or greater than δ_z,δ_r. The reason is that all the solutions we constructed for $r_g \ll \delta_z$,δ_r will still be solutions for the special cases of field-aligned electrons in the solution set that is valid for $r_g > \sim\delta_z$, δ_r. Therefore a looser bound for the width and amplitude is expected when the perpendicular motion is included. In other words, the bounding curves in Figures 9 and 10 would be shifted higher up and toward the left (smaller widths), and hence the observed widths and amplitudes would be even farther away from the bounding curve for solutions that can handle $r_g > \sim\delta_z$, δ_r.

8. Discussion

[33] The data-theory comparison in the previous section demonstrated the accessibility of electron holes that dwell deep inside the allowed space. The fact that these electron holes were detected as coherent structures indicates that their lifetime is long enough for them to remain coherent during their transit of the antennas. The questions of accessibility and stability of these loosely constrained electron holes are thus answered by the observations and data-theory comparison to certain extent. In this section we discuss the possible impact of the existence of these loosely constrained electron holes.

[34] The confirmed accessibility and stability of loosely constrained electron holes first opens up a rich mutual

interaction spectrum. For classical solitons, due to the 1-1 width-amplitude relation and the infinite conservation laws contained in their governing equations, they can only pass through each other retaining their original identities after encounter [*Drazin*, 1983]. In other words, there are no possibilities of giving rise to new solitons with different widths and amplitudes while satisfying the infinite conservation laws when solitons encounter each other. The same cannot be said for loosely constrained electron holes. The inequality width-amplitude relation of phase space holes dictates many more degrees of freedom than have classical solitons. The continuous allowed range of widths and amplitudes leads to a much richer spectrum for mutual interaction of electron holes, including complete coalescence, passing through retaining original identities, and anything in between (partial merging). Some of these possibilities have been observed in laboratory experiments [*Lynov et al.*, 1979; *Saéki et al.*, 1979] as well as simulations [*Omura et al.*, 1996].

[35] Loosely constrained electron holes can get excited much more easily than do classical solitons, again owing to their inequality width-amplitude relation. As a consequence, electron holes are more likely to play important roles in shaping the bulk properties of the plasma medium such as electrical resistivity and thermal conductivity. In a system with certain fluctuation level and different fluctuation lengths, phase-space holes can be accessed more easily since for a fixed amplitude there is a wide range of allowed widths. This is opposed to the case for solitons where the width must match the amplitude exactly. We therefore envision that in turbulent systems loosely constrained phase-space holes may be spontaneously generated even in the absence of two-stream or current-driven instabilities. The spontaneous generation of loosely constrained holes and their subsequent mutual interaction may dominate the transport properties of the turbulence. Considering that many plasma boundaries in space are characterized by fluctuations of a wide spectrum of scales and that electrostatic solitary waves are observed at plasma boundaries [*Matsumoto et al.*, 1994; *Bale et al.*, 1998; *Williams et al.*, 2005], we surmise that the birth and decay of phase-space holes would make important influences to plasma bulk properties in sustaining macroscopic boundaries.

[36] A high density of phase-space holes in the plasma could also affect the effective temperature and resistivity. At the vicinity of the solitary waves, passing particles are accelerated and, together with trapped particles, form spatially localized counterstreaming beams (Figure 8) which would have been unstable if there were no self-consistent collective field (bipolar electric field) to sustain them. The counterstreaming beams increase the velocity spread to significantly higher than that for the ambient plasma, resulting in a higher effective temperature (heating). Moreover, particle trapping will prevent particles from free acceleration by applied electric fields and regulate the electric current. The high excitation probability of these solitary waves can thus lead to finite resistivity that is required for magnetic reconnection to occur in collisionless plasmas. This view seems to be supported by recent space observations of electrostatic solitary waves in regions where magnetic reconnection occurs [*Drake et al.*, 2003; *Matsumoto et al.*, 2003].

9. Summary and Conclusion

[37] We have discussed the basic characteristics of electron holes including the underlying reason for them to have an inequality width-amplitude relation and how the inequality is modified by inclusion of ion dynamics, finite perpendicular size, and finite hole velocity. The allowed width-amplitude space shrinks for larger electron to ion temperature ratio, smaller perpendicular size, and larger hole velocity. The quantitative knowledge of how the width-amplitude inequality is modified by the above parameters enables us to make comparison to electron hole observations reported by *Franz et al.* [2005] and to demonstrate that their observations present the first experimental evidence of the inequality aspect. The capability of the Polar Plasma Wave Instrument to measure small electric field amplitudes is critical in probing the inequality aspect, as the farther away from the bounding curve and deeper into the allowed parameter space, the smaller electric field amplitudes of the electron holes. The existence of these loosely constrained electron holes opens up the possibility that they may be easily accessed by turbulent fluctuations and play important roles in transport and electrical conductivity in collisionless plasma processes such as magnetic reconnection and boundary formation.

[38] **Acknowledgments.** The authors would like to acknowledge J. Scudder for providing Hydra plasma data. The research performed by L.-J. Chen at the University of Iowa was supported by NSF ATM 03-27450. J. Pickett was supported by NASA/GSFC under contract NAS5-30371 and grants NAG5-7943 and NAG5-11942. P. Kintner and J. Franz were supported by NSF grant ATM-0105363 and by the University of Iowa under subcontracts V83923 and V400008333.

[39] Shadia Rifai Habbal thanks Andre Mangeney and another referee for their assistance in evaluating this paper.

References

Bale, S. D., P. J. Kellogg, D. E. Larson, R. P. Lin, K. Goetz, and R. P. Lepping (1998), Bipolar electrostatic structures in the shock transition region: Evidence of electron phase space holes, *Geophys. Res. Lett.*, *25*, 2929.

Behlke, R., M. André, S. D. Bale, J. S. Pickett, C. A. Cattell, E. A. Lucek, and A. Balogh (2004), Solitary structures associated with short large-amplitude magnetic structures (SLAMS) upstream of the Earth's quasi-parallel bow shock, *Geophys. Res. Lett.*, *31*, L16805, doi:10.1029/2004GL019524.

Bernstein, I. B., J. M. Greene, and M. D. Kruskal (1957), Exact nonlinear plasma oscillations, *Phys. Rev.*, *108*, 546.

Bohm, D., and E. P. Gross (1949), Theory of plasma oscillations, *Phys. Rev.*, *75*, 1851.

Boström, R., et al. (1988), Characteristics of solitary waves and double layers in the magnetospheric plasma, *Phys. Rev. Lett.*, *61*, 82.

Bounds, S., R. Pfaff, S. Knowlton, F. Mozer, M. Temerin, and C. Kletzing (1999), Solitary potential structures associated with ion and electron beams near 1 R_E altitude, *J. Geophys. Res.*, *104*, 28,709.

Cattell, C. A., J. Dombeck, J. R. Wygant, M. K. Hudson, F. S. Mozer, M. A. Temerin, W. K. Peterson, C. A. Kletzing, and C. T. Russell (1999), Comparisons of Polar satellite observations of solitary wave velocities in the plasma sheet boundary and the high altitude cusp to those in the auroral zone, *Geophys. Res. Lett.*, *26*, 425.

Cattell, C. A., C. Neiman, J. Dombeck, J. Wygant, C. A. Kletzing, W. K. Peterson, F. S. Mozer, and M. André (2003), Large amplitude solitary waves in and near the Earth's magnetosphere, magnetopause and bow-shock: Polar and Cluster observations, *Nonlinear Proc. Geophys.*, *10*, 13.

Chen, L.-J. (2002), Bernstein-Greene-Kruskal solitary waves in collisionless plasma, Ph.D. thesis, Univ. of Wash., Seattle.

Chen, L.-J., and G. K. Parks (2002a), BGK electron solitary waves in 3D magnetized plasma, *Geophys. Res. Lett.*, *29*(9), 1331, doi:10.1029/2001GL013385.

Chen, L.-J., and G. K. Parks (2002b), BGK electron solitary waves: 1D and 3D, *Nonlinear Proc. Geophys.*, *9*, 111.

Chen, L.-J., D. J. Thouless, and J.-M. Tang (2004), Bernstein-Greene-Kruskal solitary waves in three-dimensional magnetized plasma, *Phys. Rev. E*, *69*, 055,401(R).

Chen, L.-J., D. J. Thouless, and J. S. Pickett (2005), How weak can the magnetic field be for three-dimensional Bernstein-Greene-Kruskal solitary waves to exist?, *Phys. Plasmas*, in press.

Debye, P., and E. Hückel (1923), Zur theorie der elektrolyte, *Physik. Zeits.*, *24*, 185.

Drake, J. F., M. Swisdak, C. Cattell, M. A. Shay, B. N. Rogers, and A. Zeiler (2003), Formation of electron holes and particle energization during magnetic reconnection, *Science*, *299*, 873.

Drazin, P. G. (1983), *Solitons*, Cambridge Univ. Press, New York.

Ergun, R. E., C. W. Carlson, J. P. McFadden, F. S. Mozer, L. Muschietti, and I. Roth (1998), Debye-scale plasma structures associated with magnetic-field-aligned electric fields, *Phys. Rev. Lett.*, *81*, 826.

Ergun, R. E., C. W. Carlson, L. Muschietti, I. Roth, and J. P. McFadden (1999), Properties of fast solitary structures, *Nonlinear Proc. Geophys.*, *6*, 187.

Franz, J. R. (2000), A study of electron phase-space holes in the polar magnetosphere, Ph.D. thesis, Cornell Univ., Ithaca, N. Y.

Franz, J. R., P. M. Kintner, and J. S. Pickett (1998), Polar observations of coherent electric field structures, *Geophys. Res. Lett.*, *25*, 1277.

Franz, J. R., P. M. Kintner, C. E. Seyler, J. S. Pickett, and J. D. Scudder (2000), On the perpendicular scale of electron phase space holes, *Geophys. Res. Lett.*, *27*, 169.

Franz, J. R., P. M. Kintner, J. S. Pickett, and L.-J. Chen (2005), Properties of small amplitude electron phase-space holes observed by Polar, *J. Geophys. Res.*, *110*, A09212, doi:10.1029/2005JA011095.

Ghosh, S. S., and G. S. Lakhina (2004a), Anomalous width variation of rarefactive ion acoustic solitary waves in the context of auroral plasmas, *Nonlinear Proc. Geophys.*, *11*, 219.

Ghosh, S. S., and G. S. Lakhina (2004b), *Positive Amplitude Electron Acoustic Solitary Waves in Auroral Plasma*, COSPAR, Paris.

Gurnett, D. A., and A. Bhattacharjee (2005), *Introduction to Phasma Physics With Space and Laboratory Applications*, Cambridge Univ. Press, New York.

Gurnett, D. A., et al. (1995), The Polar plasma wave instrument, *Space Sci. Rev.*, *71*, 597.

Jackson, J. D. (1990), *Classical Electrodynamics*, John Wiley, Hoboken, N. J.

Kojima, H., Y. Omura, H. Matsumoto, K. Miyaguti, and T. Mukai (1999), Characteristics of electrostatic solitary waves observed in the plasma sheet boundary: Statistical analysis, *Nonlinear Proc. Geophys.*, *6*, 179.

Krasovsky, V. L., H. Matsumoto, and Y. Omura (1997), Bernstein-Greene-Kruskal analysis of electrostatic solitary waves observed with Geotail, *J. Geophys. Res.*, *102*, 22,131.

Krasovsky, V. L., H. Matsumoto, and Y. Omura (2003), Electrostatic solitary waves as collective charges in a magnetospheric plasma: Physical structure and properties of bernstein-greene-kruskal (BGK) solitons, *J. Geophys. Res.*, *108*(A3), 1117, doi:10.1029/2001JA000277.

Krasovsky, V. L., H. Matsumoto, and Y. Omura (2004), Effect of trapped-particle deficit and structure of localized electrostatic perturbations of different dimensionality, *J. Geophys. Res.*, *109*, A04217, doi:10.1029/2003JA010198.

Lynov, J. P., P. Michelsen, H. L. Pécseli, and K. S. J. Juul Rasmussen (1979), Observations of solitary structures in a magnetized plasma loaded wave guide, *Phys. Scr.*, *20*, 328.

Mangeney, A., et al. (1999), Wind observations of coherent electrostatic waves in the solar wind, *Ann. Geophys.*, *17*, 307.

Matsumoto, H., H. Kojiima, T. Miyatake, Y. Omura, M. Okada, I. Nagano, and M. Tsutsui (1994), Electrostatic solitary waves (ESW) in the magnetotail: BEN wave forms observed by GEOTAIL, *Geophys. Res. Lett.*, *21*(25), 2915.

Matsumoto, H., X. H. Deng, H. Kojima, and R. R. Anderson (2003), Observation of electrostatic solitary waves associated with reconnection on the dayside magnetopause boundary, *Geophys. Res. Lett.*, *30*(6), 1326, doi:10.1029/2002GL016319.

McFadden, J. H., C. W. Carlson, R. E. Ergun, F. S. Mozer, L. Muschietti, I. Roth, and E. Moebius (2003), Fast observations of ion solitary waves, *J. Geophys. Res.*, *108*(A4), 8018, doi:10.1029/2002JA009485.

Morse, R. L., and C. W. Nielson (1969), One-, two-, and three-dimensional numerical simulation of two-beam plasma, *Phys. Rev. Lett.*, *23*, 1087.

Mozer, F. S., R. E. Ergun, M. Temerin, C. Cattell, J. Dombeck, and J. Wygant (1997), New features of time domain electric-field structures in the auroral acceleration region, *Phys. Rev. Lett.*, *79*, 1281.

Muschietti, L., R. E. Ergun, I. Roth, and C. W. Carlson (1999a), Phase-space electron holes along magnetic field lines, *Geophys. Res. Lett.*, *26*(8), 1093.

Muschietti, L., R. E. Ergun, I. Roth, and C. W. Carlson (1999b), Correction to "Phase-space electron holes along magnetic field lines," *Geophys. Res. Lett.*, *26*, 1689.

Muschietti, L., I. Roth, R. E. Ergun, and C. W. Carlson (1999c), Analysis and simulation of BGK electron holes, *Nonlinear Proc. Geophys.*, *6*, 211.

Muschietti, L., I. Roth, C. W. Carlson, and R. E. Ergun (2000), Transverse instability of magnetized electron holes, *Phys. Rev. Lett.*, *85*, 94.

Muschietti, L., I. Roth, C. W. Carlson, and M. Berthomier (2002), Modeling stretched solitary waves along magnetic field lines, *Nonlinear Proc. Geophys.*, *9*, 101.

Omura, Y., H. Matsumoto, and H. Kojima (1996), Electron beam instabilities as generation mechanism of electrostatic solitary waves in the magnetotail, *J. Geophys. Res.*, *101*, 2685.

Pickett, J. S., J. D. Menietti, D. A. Gurnett, B. Tsurutani, P. M. Kintner, E. Klatt, and A. Balogh (2003), Solitary potential structures observed in the magnetosheath by the Cluster spacecraft, *Nonlinear Proc. Geophys.*, *10*, 3.

Pickett, J. S., L.-J. Chen, S. W. Kahler, O. Santolik, D. A. Gurnett, B. T. Tsurutani, and A. Balogh (2004a), Isolated electrostatic solitary structures observed throughout the Cluster orbit: Relationship to magnetic field strength, *Ann. Geophys.*, *22*, 2515.

Pickett, J. S., et al. (2004b), Isolated electrostatic structures observed in the auroral zone: the Cluster multi-spacecraft perspective, *Nonlinear Proc. Geophys.*, *11*, 183.

Saéki, K., P. Michelsen, H. L. Pécseli, and J. J. Rasmussen (1979), Formation and coalescence of electron solitary holes, *Phys. Rev. Lett.*, *42*, 501.

Schamel, H. (1979), Theory of electron holes, *Phys. Scr.*, *20*, 336.

Schamel, H. (1986), Electron holes, ion holes and double layers, *Phys. Rep.*, *140*, 161.

Temerin, M., K. Cerny, W. Lotko, and F. S. Mozer (1982), Observations of double layers and solitary waves in the auroral plasma, *Phys. Rev. Lett.*, *48*, 1175.

Tsurutani, B. T., J. K. Arballo, G. S. Lakhina, C. M. Ho, B. Buti, J. S. Pickett, and D. A. Gurnett (1998), Plasma waves in the dayside polar cap boundary layer: Bipolar and monopolar electric pulses and whistler mode waves, *Geophys. Res. Lett.*, *25*, 4117.

Turikov, V. A. (1984), Electron phase-space holes as localized BGK solutions, *Phys. Scr.*, *30*, 73.

Williams, J. D., et al. (2005), Electrostatic solitary structures associated with the November 10, 2003 interplanetary shock at 8.7 AU, *Geophys. Res. Lett.*, doi:10.1029/2005GL023079, in press.

L.-J. Chen, D. Gurnett, and J. Pickett, Department of Physics and Astronomy, University of Iowa, Iowa City, IA 52242, USA. (li-jen-chen@uiowa.edu)

J. Franz and P. Kintner, School of Electrical Engineering, Cornell University, Ithaca, NY 14850, USA.